SEISMIC RESPONSE EVALUATION OF LATTICE SHELL ROOFS USING AMPLIFICATION FACTORS

T. TAKEUCHI[1], T. OGAWA[2], T. KUMAGAI[3]

[1]Assoc. Prof., Tokyo Institute of Technology, O-okayama 2-12-1-M1-29, Meguro-ku, Tokyo, Japan, ttoru@arch.titech.ac.jp
[2]Prof., Tokyo Institute of Technology, O-okayama 2-12-1-M1-29, Meguro-ku, Tokyo, Japan
[3]Assist. Prof., Tokyo Institute of Technology, O-okayama 2-12-1-M1-29, Meguro-ku, Tokyo, Japan

Editor's Note: Manuscript submitted 27 February 2007; revision received 1 October 2007. This paper is open for written discussion, which should be submitted to the IASS Secretariat no later than August 2008.

ABSTRACT

Seismic response of lattice shell roofs with substructures is complicated, because these roofs have large numbers of parallel vibration modes, and their amplitude changes drastically along the rise/span ratios and the stiffness ratios between domes and substructures. Under limited condition, however, their response characteristics are considered to become relatively simple. In this paper, simple response evaluation method of domes and cylindrical shell roofs with substructures are proposed using response amplification factors approach. Firstly, the response characteristics of raised roofs with various depth/span ratios and substructure stiffness are numerically discussed with simple arch model. Then response of lattice domes and cylindrical shell roofs are investigated, and simple acceleration response evaluation method using response amplification factors is delivered. The proposed method can be used as equivalent static loads for design, and compared with precise analyses with CQC method.

Keywords: *Seismic Response, Arch, Lattice Dome, Cylindrical Lattice Shell, Equivalent Static Loads*

1. INTRODUCTION

Raised dome or shells under horizontal seismic input are known to cause vertical response together with horizontal response, and applying normal horizontal seismic loads are often dangerous in seismic design. (Figure1). Their characteristics are quite complicated because such roofs normally have large numbers of parallel vibration modes. Such vibration modes are randomly oscillated by their supporting structures, and their amplitudes change drastically along the relationship between the roofs and supporting substructures. To predict these response, large numbers of researches are carried out. For example, Kato and Nakazawa were modeled dome roof structures in parallel mass model, and proposed response evaluation method using these models [1]. In these studies, they have indicated the numbers of oscillated modes are reduced where the out-of-plane stiffness are increased, and proposed the ultimate-state design method using the push-over analyses [2].

For cylindrical shell roofs, S.Yamada and others has carried out various studies [3]. They are analyzed large numbers of cylindrical shells with various boundary conditions, and proposed equivalent static loads for design using maximum strain-energy concept. Such equivalent static loads are quite useful for practical design, because normal buildings are designed with equivalent static loads for seismic design. However, the effects of substructures on the equivalent static loads are yet made clear in those studies.

For the effects of substructures on roof response are primarily studied by M.Yamada using double degree of mass model [4]. They also proposed the equivalent static loads for arches using parametric time-history analyses [5], however, effects of rise/span ratio or relationship between substructures were not clearly explained.

In this paper, the basic response characteristics of raised roof are firstly explained using simple arch model. Their maximum responses are expressed by simple equations with parameters of half subtended angle and own-period ratio between the roof and substructures. With these studies, response evaluation method using amplification factors are proposed. The concept is applied to spherical domes and cylindrical shells respectively, and common design method with different amplification factors is proposed, followed by verification of their accuracies where they are used as equivalent static loads.

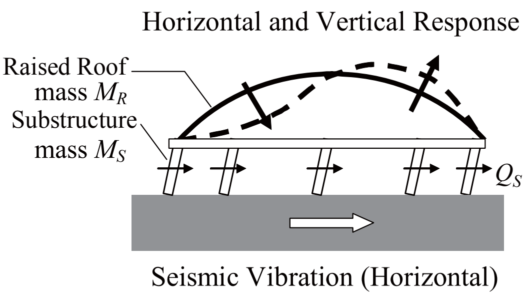

Figure 1. *Seismic Response of Raised Roof*

2. RESPONSE EVALUATION WITH SIMPLE ARCH MODEL

Firstly, response characteristics of raised roofs are explained theoretically using simple arch model as shown in Figure 2. This model has 3 spring hinges and rigid axial stiffness. From the geometric relationship in Figure 2, the asymmetrical deflection mode vector is expressed as the following.

$$\mathrm{u}^T = [\delta_{1x}, \delta_{1y}, \delta_{2x}, \delta_{2y}, \delta_{3x}, \delta_{3y}]$$
$$= u\left[\sin\frac{3}{4}\theta, -\cos\frac{3}{4}\theta, 2\sin\frac{\theta}{4}, 0, \sin\frac{3}{4}\theta, \cos\frac{3}{4}\theta\right] \tag{1}$$

Where, u=$2R\alpha\sin(\theta/4)$…(1a). Then, participation factor for this mode β_{R1}, and effective mass M_{R1} become as follows.

$$\beta_{R1} = \frac{\mathbf{u}^T\mathbf{m}\mathbf{I}_x}{\mathbf{u}^T\mathbf{m}\mathbf{u}} = \frac{2\left(\sin\frac{3}{4}\theta + \sin\frac{\theta}{4}\right)}{u\left(2 + 4\sin^2\frac{\theta}{4}\right)} = \frac{\sin\frac{3}{4}\theta + \sin\frac{\theta}{4}}{u\left(1 + 2\sin^2\frac{\theta}{4}\right)} \tag{2}$$

$$M_{R1} = \frac{(\mathbf{u}^T\mathbf{m}\mathbf{I}_x)^2}{\mathbf{u}^T\mathbf{m}\mathbf{u}} = \frac{2m\left(\sin\frac{3}{4}\theta + \sin\frac{\theta}{4}\right)^2}{1 + 2\sin^2\frac{\theta}{4}} \tag{3}$$

Where, **m** is mass matrix whose diagonal elements are m_{ii}=[m,m,m,m,m,m], $\mathbf{I}_x$ is vector whose horizontal elements are 1 and other elements are 0.

The rest of effective mass M_{R2} can be calculated by removing M_{R1} from the total mass M_R =3m. M_{R2} is given by all other vibration modes with axial deformation, which become identical to the ground motion because the axial stiffness is infinity.

$$M_{R2} = M_R - M_{R1} = 3m\left(1 - \frac{2m\left(\sin\frac{3}{4}\theta + \sin\frac{\theta}{4}\right)^2}{3\left(1 + 2\sin^2\frac{\theta}{4}\right)}\right) \tag{4}$$

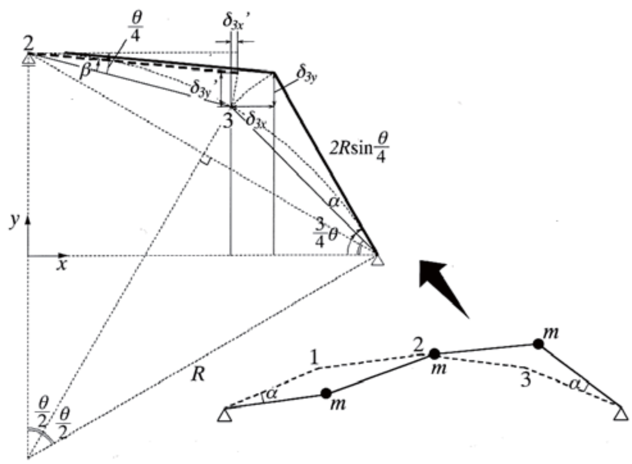

Figure 2. *3-hinged Arch Model*

When θ decreases, M_{R2} increases compared with M_{R1}, and M_{R2} become 100% when θ=0. Referring [6], maximum response $\boldsymbol{a}_R$ is estimated by calculating SRSS between the vibration mode shown in Figure 2 and ground motion.

$$a_R = [a_{1x}, a_{1y}, a_{2x}, a_{2y}, a_{3x}, a_{3y}]^T$$
$$= \sqrt{(S_{AP}\beta_{R1}\mathbf{u})^2 + \left(S_{Ag}\mathbf{I}_x\frac{M_{R2}}{M_R}\right)^2} \tag{5}$$

For understanding the characteristics of response, normalized seismic spectrum is useful for verification. In this paper, artificial seismic spectrum following [7] as shown in Figure 3 is defined as BRI-L1 and used for evaluation. In Figure 3, earthquake records normalized their maximum velocity as 25cm/sec are also shown. This figure shows the BRI-L1 almost covers these earthquake records. BRI-L1 is given in the following equations.

$$S_A(T)=\begin{cases}200D_h & (0\le T<0.04)\\ 200D_h(T/0.04)^{\log 3/\log 4.5} & (0.04\le T<0.18)\\ 600D_h & (0.18\le T<\pi/6)\\ 100\pi D_h/T & (\pi/6\le T<5)\\ 100\sqrt{5}\pi D_h/T^{3/2} & (5\le T<10)\end{cases} \quad (6)$$

$$D_h=\sqrt{(1+97h_0)/(1+97h)}=1.411 \quad (h_0=0.05,\ h=0.02)$$

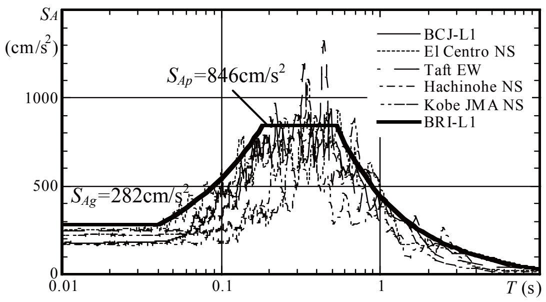

Figure 3. *Design Acceleration Spectrum*

Eq.(5) is based on the condition that the natural period of asymmetrical vibration mode is placed in the constant-acceleration zone S_{Ap} in Figure 3. Response amplitude factor is estimated as $\boldsymbol{a}_R/S_{Ag}$ as following, with the condition of $S_{Ap}=3S_{Ag}$.

$$\frac{\boldsymbol{a}_R}{S_{Ag}}=\sqrt{\left(\frac{S_{Ap}}{S_{Ag}}\beta_{R1}\mathbf{u}\right)^2+\left(\mathbf{I}_x\frac{M_{R2}}{M_R}\right)^2}=\sqrt{(3\beta_{R1}\mathbf{u})^2+\left(\mathbf{I}_x\frac{M_{R2}}{M_R}\right)^2} \quad (7)$$

Calculated amplification factors by eq.(7) are shown in Figure 4, compared with M.Yamada's proposal [5] and results of response spectrum evaluation with CQC method which is confirmed to be consistent with time-history analyses in [8] using detailed arch roof models [10].

Effects of substructures are estimated using SDOF model and equivalent DDOF model as shown in Figure 5(a) and (b), respectively. Maximum acceleration obtained from response spectrum and SDOF model is defined as A_{eq}. Also in DDOF, defining effective mass of the roof and the substructure as $M_{Req}=M_{R1}$, $M_{Seq}=M_S+M_{R2}$ (where, $M_{R1}+M_{R2}=M_R$), maximum response of DDOF is calculated by SRSS of two modes obtained by eigen mode analysis, as follows.

$$\boldsymbol{a}_2=[A_S,A_R]^T=\sqrt{(S_{A1}\beta_1\mathbf{u})^2+(S_{A2}\beta_2\mathbf{u})^2} \quad (8)$$

Maximum response of upper mass A_R is obtained from eq.(8). Then S_{Ap} in eq.(7) is replaced by A_R, and S_{Ag} is replaced by A_{eq}, amplification factor is calculated as follows, divided by A_{eq}.

$$\frac{\boldsymbol{a}_R}{A_{eq}}=\sqrt{\left(\frac{A_R}{A_{eq}}\beta_{R1}\mathbf{u}\right)^2+\left(\mathbf{I}_x\frac{M_{R2}}{M_R}\right)^2} \quad (9)$$

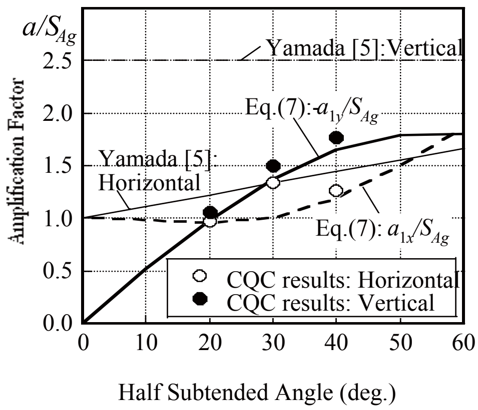

Figure 4. *Amplification Ratios for Arch Roof*

Calculated factors are the functions of θ, and natural period ratio between SDOF and the roof $R_T=T_{eq}/T_R$. Horizontal component a_{RH}/A_{eq} and vertical component a_{RV}/A_{eq} in eq.(9) are shown in Figure 5(c) and (d), along R_T. Also the results of CQC method with detailed arch models are shown in marks. The proposed design factors are consistent with CQC results. These amplification factors are also affected by the mass ratio $R_M=M_{eq}/M_R$, as in Figure 6. Where R_M values are large, amplification factors excite around R_T =1, because of resonance between the roof and the substructure.

Using these equations, the maximum acceleration in the raised roofs can be evaluated by the following process, as in Figure 7.

1. Calculate natural period in SDOF model T_{eq}, and evaluate A_{eq} with response spectrum.
2. Evaluate the natural period of asymmetric one-

wave mode of the roof T_D, and calculate $R_T = T_{eq}/T_D$.

3. Calculate amplification factors ($F_H = a_{RH}/A_{eq}$, $F_V = a_{RV}/A_{eq}$), and evaluate A_H and A_V with distribution functions.
4. Evaluate deflections and member forces by estimating A_H and A_V as equivalent static load coefficient.

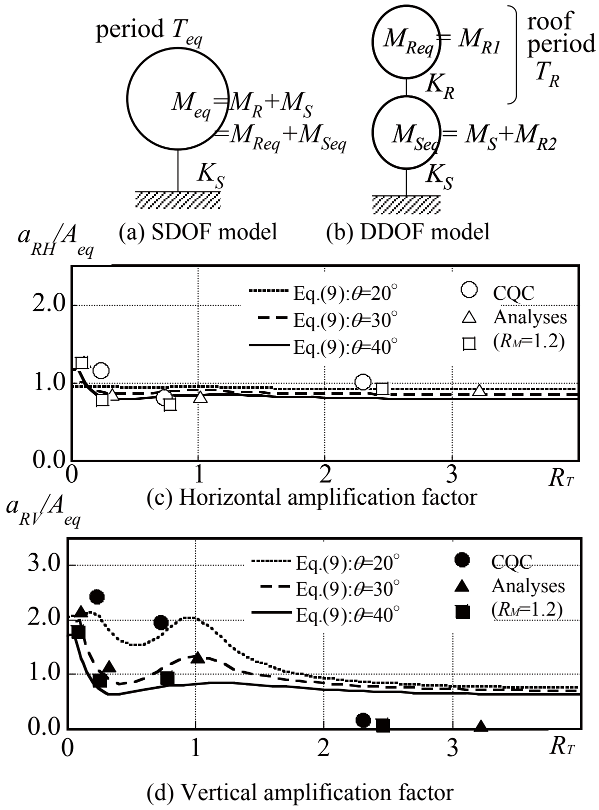

Figure 5. *Amplification Ratios with R_T*

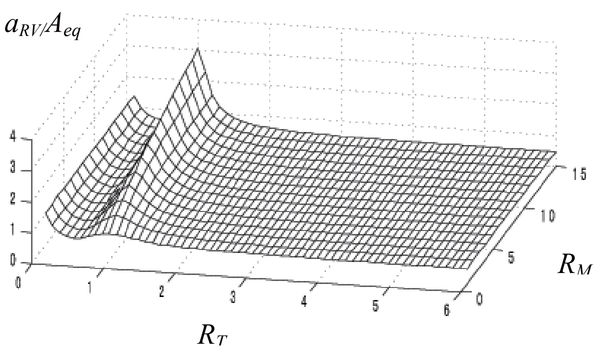

Figure 6. *Amplification Ratios with R_M (θ=30°)*

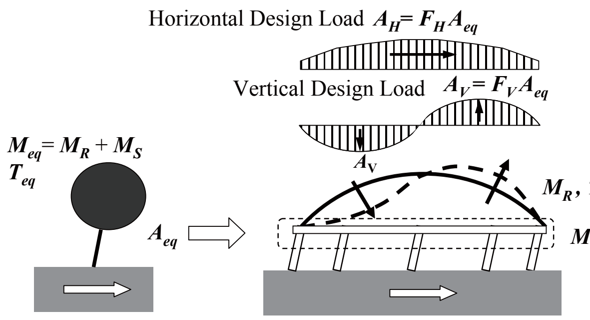

Figure 7. *Response Evaluation with Amplification Factors*

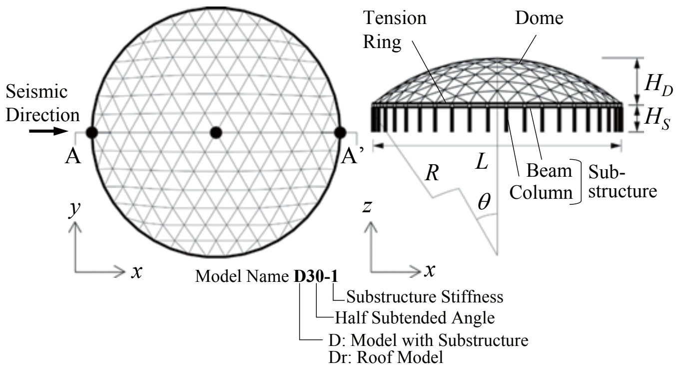

Figure 8. *Lattice Dome Model with Substructure*

3. RESPONSE CHARACTERISTICS OF DOME

The proposed concept is applied to spherical lattice domes and amplification factors are researched in the following. The analysis models are rigidly jointed lattice domes with substructure as shown in Figure 8, and the dimension of the domes are given in Table 1. The dome span is 60m and the rises of the domes are varied as the half subtended angle of 20, 30 and 40 degrees. The substructure is moment frames composed of pipe members, column's base being supported by pin. Tension ring is placed at the boundary of the domes, and the joints between the tension ring and the substructure are pin connected. The analysis models are named as D_r30 for θ= 30 degrees without substructure, and D30-(substructure stiffness ratio) with substructure. The members of the domes are tubular sections as shown in Table 2, being designed elastic against the dead load of uniform 1.18 kN/m^2. The members of the substructure are designed so that the story drifts under the horizontal load with the base shear coefficient C_0=0.3 is less than 1/200. In the dome, the line connecting node A to A' through O in Figure 8 is called as the ridge of the dome.

Table 1. *Size of Dome Models*

Half Subtended Angle θ(deg.)	20.0	30.0	40.0
Span of the Dome L (cm)	6000		
Radius of the Dome R (cm)	8771	6000	4667
Rise of the Dome H_D (cm)	529	804	1092
Column Height H_S (cm)	600		
Ridge Member Length l (cm)	510	523	543

Table 2. *Size of Dome Models*

	Size of Ridge Members			Tension Rings	Column
H.S. Angle θ	20°	30°	40°		
Slenderness Ratio λ	90.6∼93.4	91.8∼93.2	94.9∼95.8	21.2	18.9
Diameter D (cm)	16.52			60.96	91.44
Thickness t (cm)	0.60∼1.10	0.40∼0.65	0.35∼0.50	1.27	1.60
Section Area A (cm^2)	30.01∼53.29	20.26∼32.41	17.78∼25.16	238	452
Moment of Inertia I (cm^4)	952∼1592	658∼1020	581∼808	106000	456000
Elastic Modulus E (kN/mm^2)	206				

Previous studies [9] indicate double-layer domes show simpler vibration modes than single-layer domes. So the roof models without substructures with increased out-of-plane bending stiffness by 10 times are set as d10, 100 times as d100, and effects on vibration modes are studied. As indicated in Table 3, d10 series and d100 series meet the double layer lattice dome of depth/span ratio of about 1/170 and 1/50, respectively.

Table 3. *Depth/Span Ratio (d/L)*

Model	θ=20°	θ=30°	θ=40°
d1	-	-	-
d10	1/ 172	1/ 169	1/ 168
d100	1/ 54	1/ 53	1/ 53

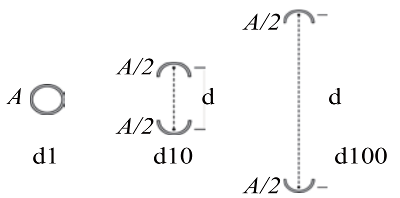

The numbers of main vibration modes for each series are shown in Figure 9. The numbers of modes satisfying their total effective mass ratio as 90% of total is decreased when their out-of-plane stiffness are increased from d1 to d100. In these condensed modes, 4 modes of asymmetrical 1 wave (O1), asymmetrical 2 wave (O2), asymmetrical 2.5 wave (O2.5), and in-plane (I) shown in Figure10 are commonly appears, and more than 80% of effective mass ratio is covered with these 4 modes. The roof itself has the O1 vibration mode with natural period of 0.3 sec, and 2.5 mode with 0.12 sec. According to the stiffening of the substructure from D30-0.1 to D30-100, excited mode of the roof shifts from O1 to O2.5. These 4 modes are called as principal 4 modes in this paper. When depth/span ratio of the dome reaches 1/50 or more, major vibration modes are condensed to the principal modes as in Figure 10, and response characteristics also are considered to be simplified. Under this conditions, effects of substructure stiffness are studied. By fixing out-of-plane stiffness as d100 series, horizontal stiffness of substructures is multiplied by 0.1, 10, and 100. The model with 30 degree half subtended angle with 10 times substructure stiffness is called F30-10, for example. In Table 4, the equivalent natural period T_{eq} of SDOF model, estimating the whole dome and upper half of substructure as single mass, are shown. In Figure 11, effects of substructure stiffness and major modes whose total effective mass ratio is over 90%, are shown. In this stage, all of the major vibration modes are consists of the principal 4 modes of O1, O2, O2.5 and I modes defined in Figure 10. After here, response analysis uses the principal 4 modes only, with CQC method. This method is also confirmed to be consistent with time-history analyses in the previous research [8]. With various stiffness of substructures, the vertical and horizontal acceleration responses calculated with main 4 modes for angle-30 series are shown in Figure12. The figure indicates the responses with stiff substructure (D30-100) are almost the same as roof model without substructure (D_r30). On contrary, the responses with soft substructure (D30-0.1), the sway mode controls the whole structure, horizontal acceleration almost flat and vertical response being almost disappeared. In D30-10 and D30-1, vibrations of the dome roof and the substructure interfere each other, however, their response can be evaluated as the combinations of principal 4 modes. The two peaks appearing in the vertical acceleration in D30-10 can be explained by combination of asymmetric 2 wave and 2.5 wave. The response of D30-1 is represented by asymmetric 1 wave. Thus, response spectrum analyses with principal modes are useful to understand the response characteristics.

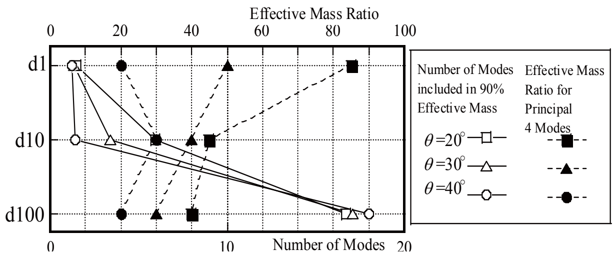

Figure 9. *Condensation of Major Modes*

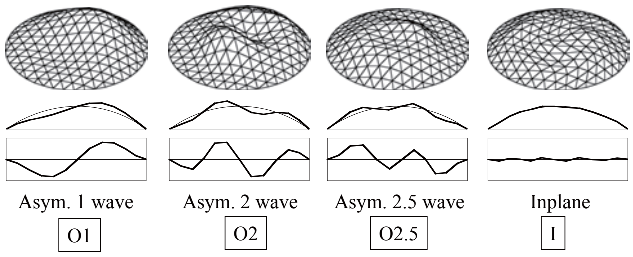

Figure 10. *Principal 4 Modes*

Table 4. *Equivalent natural Period of Substructures*

Model	θ=20°	θ=30°	θ=40°
DX-0.1	1.155 s	1.173 s	1.199 s
DX-1	0.350 s	0.355 s	0.362 s
DX-10	0.111 s	0.112 s	0.115 s
DX-100	0.035 s	0.036 s	0.036 s

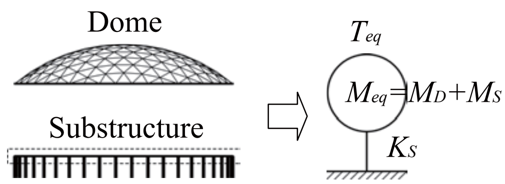

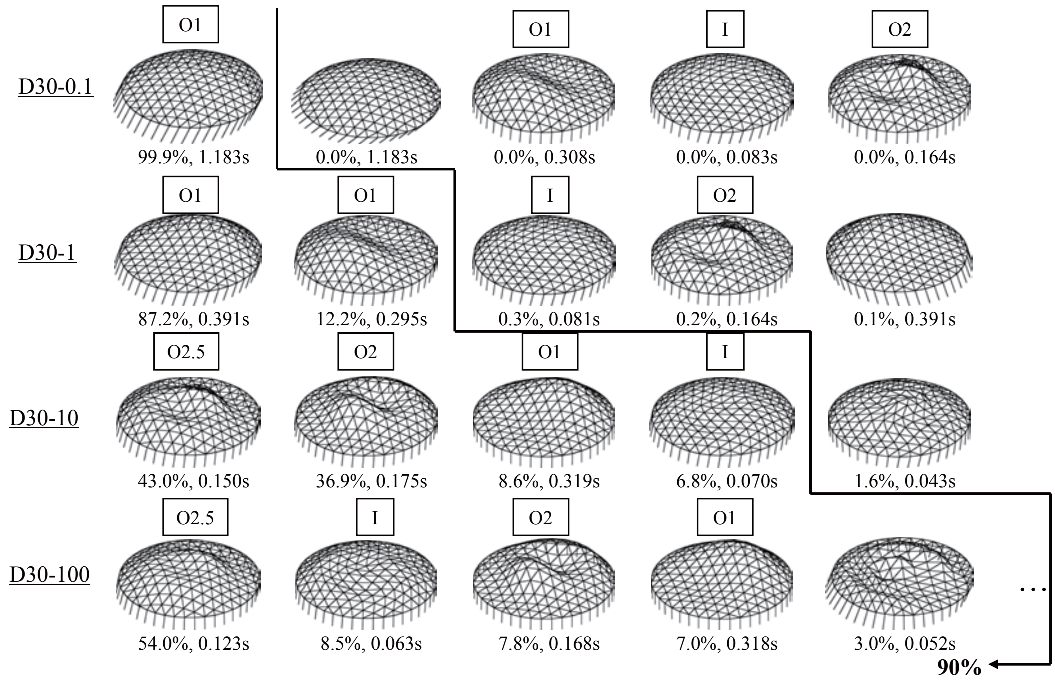

Figure 11. *Effects of Substructure Stiffness*

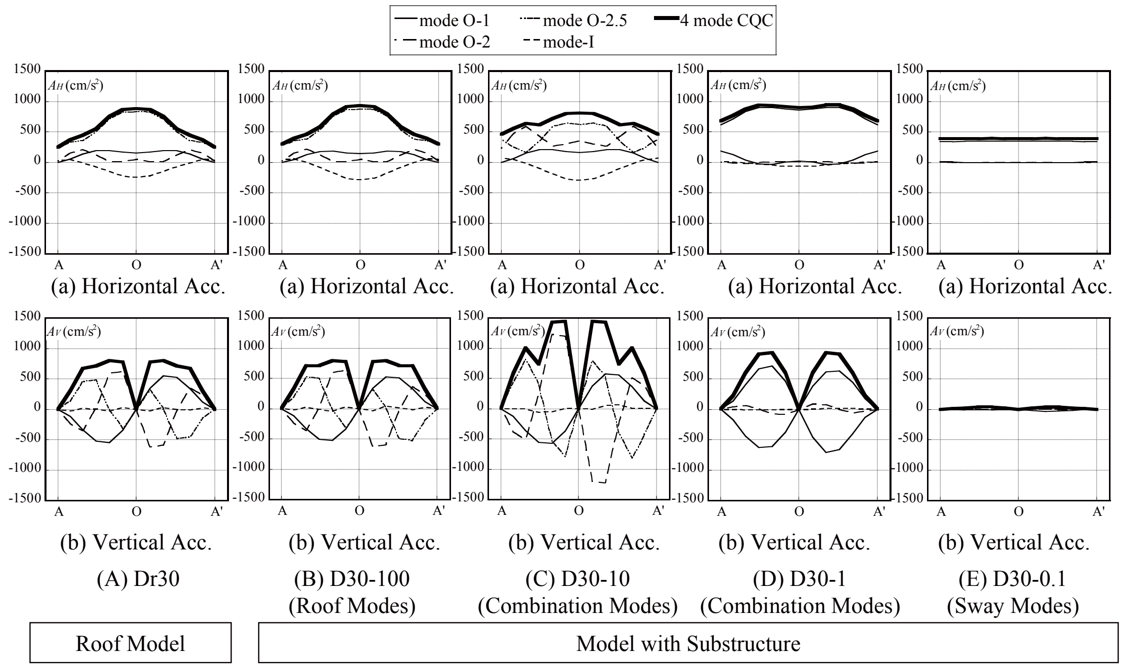

***Figure 12**.Components of Each Mode*

The first step to estimate the amplification factor is to study the effect of half subtended angle using roof model without substructures. The relationship between the maximum acceleration and half subtended angles are plotted in Figure 13. The maximum values of horizontal acceleration are almost flat regardless of the angle, and the value itself correspond to the maximum values S_{AP} in Figure 3 spectrum. The maximum values of vertical acceleration are linearly increases along the angle between 20-40 deg., and expressed as $S_{AP} \times C_V \times \theta$(rad), where C_V is constant=1.85.

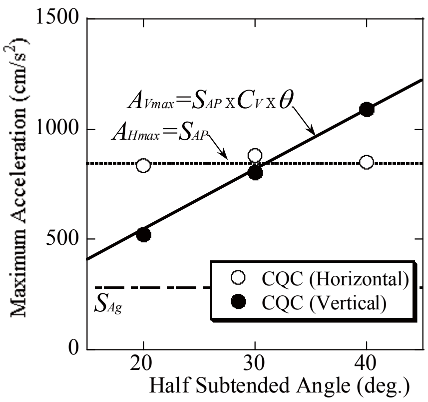

***Figure 13**. Effect of Half Subtended Angle*

In the next, amplitude effect by the substructure is evaluated. This effect is considered to be expressed as a function of R_T, and the relationship between $F_H = a_{Hmax}/A_{eq}$, $F_V = a_{Vmax}/A_{eq}$ and R_T is plotted in Figure 14. Where a_{Hmax}, a_{Vma} is maximum acceleration in the roof in horizontal and vertical directions respectively, and A_{eq} is acceleration in SDOF model. To estimate these effects, horizontal amplitude effect F_H, and vertical amplitude effect F_V is expressed as the following equations, as approximations to cover the parametric study results.

$$F_H = \begin{cases} 3 & (0 < R_T \le 5/36) \\ \sqrt{5/4R_T} & (5/36 < R_T \le 5/4) \\ 1 & (5/4 < R_T) \end{cases} \qquad (10)$$

$$F_V = \begin{cases} 3C_V\theta & (0 < R_T \le 5/16) \\ \left(\sqrt{5/R_T} - 1\right)C_V\theta & (5/16 < R_T \le 5) \\ 0 & (5 < R_T) \end{cases} \qquad (11)$$

Comparing these amplification factors with those of simple arch model in Figure 5, magnitudes in lower R_T zones are remarkable. These differences are produced by higher vibration mode amplification in roof models. It is also noted that F_H and F_V should be the function of not only R_T but R_M, however, eq.(10)(11) are expressed by R_T only, for lower R_M (=1.2) in present study. From studies, as above, the maximum acceleration distribution can be expressed as the following functions, using the coordinates in the roof.

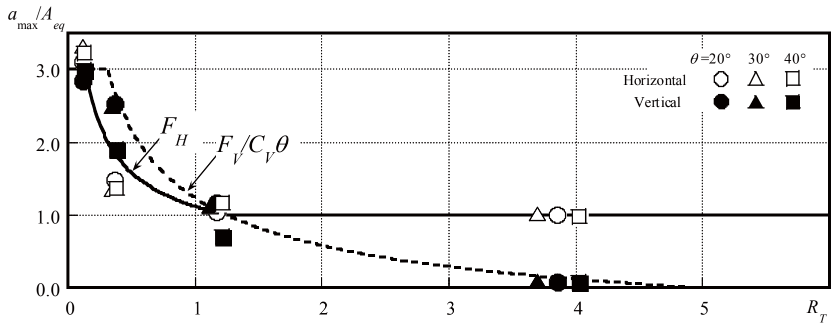

***Figure 14**. Amplification Factors for Dome*

Horizontal acceleration:

$$A_H(x,y) = A_{eq}\left\{1+(F_H-1)\cos\frac{\pi\sqrt{x^2+y^2}}{L}\right\} \qquad (12)$$

Vertical acceleration:

$$A_V(x,y) = A_{eq}F_V\frac{x}{\sqrt{x^2+y^2}}\sin\frac{\pi\sqrt{x^2+y^2}}{L} \qquad (13)$$

The comparison of above factors and CQC results are shown in Figure 15. The equivalent static loads are delivered by multiplying these accelerations with the self-weight distribution of the dome. The displacements and member forces using these equivalent static loads are also compared with CQC results in Figure 16. The results of proposed method seem consistent with those of CQC, and considered to be effective. The accuracies in member forces are relatively worse, which is caused by estimating the equivalent load distributions from the coverage of maximum accelerations. Replacing eq.(12)(13) by another distribution approach as [3] could help the improvement, however, the present accuracy is considered to be enough for practical design.

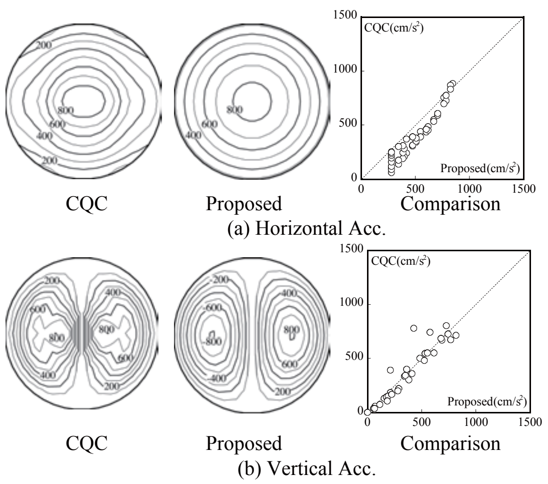

***Figure 15.** Acceleration Dstribution in Dome (Dr30)*

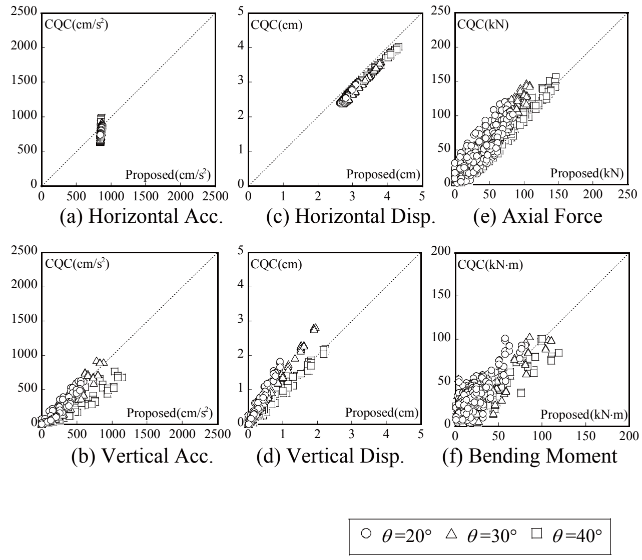

***Figure 16.** Accuracies of Proposed Static Loads (Dθ-1 series)*

4. RESPONSE CHARACTERISTICS OF CYLINDRICAL SHELL

Next, the same concept is applied to cylindrical shell roofs. The analysis models are rigidly jointed lattice shell roofs with substructure as shown in Figure 17, and the dimension of the roofs are given in Table 5. The roof spans are 36m and the rises of the roofs are varied as the half subtended angle of 20, 30 and 40 degrees. The substructures are moment frames composed of pipe members, column's base being supported by fixed. Tie beams are placed at the edge of the roofs, and the joints between the roof and the substructure are pin connected. The members of the roofs are tubular sections, being designed under uniform dead load of 1.18kN/m^2, as same as the dome models. The members of the substructure are designed so that the story drifts under the horizontal load with the base shear coefficient C_0=0.3 are less than 1/200. In the roof, the line connecting node A to A' through O in Figure 17 are called as the ridge of the roof. Then the out-of-plane stiffness of the roof members are multiplied by 10 times or 100 times, which are equal to depth/span ratios of about 1/100 or 1/30 respectively, as shown in Table 7. In the following discussions, d10 are represented. Horizontal stiffness of substructure is also multiplied by 0.1, 10, or 100 times. These analysis models are named as S(θ)-(Substructure stiffness ratio). For example, S30-10 means the roof of θ=30 degrees of half subtended angle, with depth/span ratio of 1/32, with the 10 times of substructure stiffness from the standard frame. Roofs without substructures are named as Sr series, expressed as Sr30.As same as domes, effects of substructure stiffness are studied. By fixing out-of-plane stiffness as d10 series, horizontal stiffness of substructures is changed. In Table 8, the equivalent natural period T_{eq} of SDOF model, estimating the whole roof and upper half of substructure as single mass, are shown. In Figure 18, effects of substructure stiffness and major modes whose total effective mass ratio is over 98%, are shown. In this stage, the numbers of the major vibration modes decrease along the substructure stiffness decrease, as same as domes.

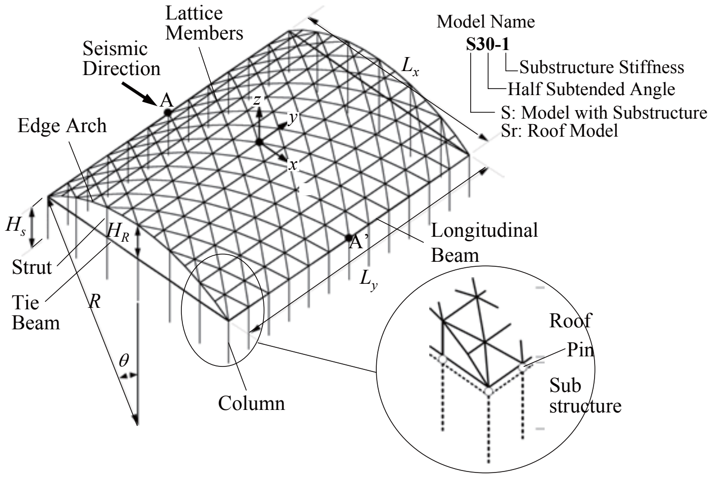

Figure 17. *Cylindrical Shell Roof Model*

Table 5 *Sizes of Shell Models*

Half Subtended Angle θ(°)	20	30	40
x-dir. Span L_x (cm)	3600		
y-dir. Span L_y (cm)	4800		
Radius of the Shell R (cm)	5263	3600	2800
Rise of the Shell H_R (cm)	317	482	655
Column Length H_S (cm)	600		

Table 6. *Member Sizes of Shell Models*

	H.S.Angle θ	Slenderness ratio λ	Diameter D (cm)	Thickness t (cm)	Section Area A (cm^2)	Moment of Inertia I (cm^4)
Lattice Members	20°	27.1～54.2	21.63	0.75	49.2	2685
	30°	35.0～70.0	16.52	0.35, 0.50	17.8, 25.2	581, 808
	40°	41.6～83.3	13.98	0.40, 0.60	17.1, 25.2	394, 566
Edge Arch		15.9	55.88	1.50	256.3	94798
Tie Beam		48.1～50.1	35.56	1.10	119.1	17695
Longitudnal Beam		11.4	101.6	2.00	625.8	776324
Strut		26.6～48.1	19.07	0.40	23.5	1023
Column		34.0	50.80	0.85	133.4	41611

Table 7. *Depth/Span Ratio (d/L)*

Model	θ=20°	θ=30°	θ=40°
d1	-	-	-
d10	1/ 78	1/ 100	1/ 120
d100	1/ 24	1/ 32	1/ 38

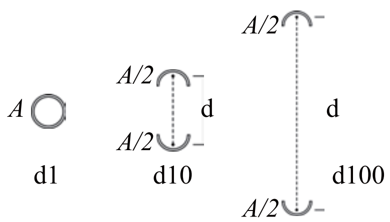

***Table 8**. Equivalent Natural Period of Substructures*

Model	θ=20°	θ=30°	θ=40°
SX-0.1	1.260 s	1.289 s	1.323 s
SX-1	0.398 s	0.408 s	0.419 s
SX-10	0.126 s	0.129 s	0.132 s
SX-100	0.040 s	0.041 s	0.042 s

With various stiffness of substructure, the vertical and horizontal acceleration responses calculated for Sr30-10-x series are shown in Figure 19. The figure indicates the responses with stiff substructure (S30-100) are almost the same as roof model without substructure (Sr30). On contrary, the responses with soft substructure (S30-0.1), the sway mode controls the whole structure, horizontal acceleration being almost flat and vertical response being almost disappeared. In S30-10 and S30-1, vibrations of the roofs and the substructure interferes each other. The response of S30-1 is represented by asymmetric 1st wave. These characteristics are similar as those of lattice domes.

For fixing the evaluation formula, the effect of half subtended angle is studied using roof model ithout substructures. The relationship between the maximum acceleration and half subtended angles are plotted in Figure 20. The maximum values of horizontal acceleration are almost flat regardless of the angle, and the value itself correspond to the maximum values of 1.5 S_{Ag} in Figure 3 spectrum.

The maximum values of vertical acceleration are linearly increases along the angle, and expressed as $S_{AP}\times C_V\times\theta$ (rad), where C_V is constant=1.33.

From these results, amplitude effect by the substructure is evaluated. The relationship between $F_H=a_{H\max}/A_{eq}$, $F_V=a_{V\max}/A_{eq}$ and R_T calculated from each models are plotted in Figure 21. To cover these effects, horizontal amplitude effect F_{RH}, and vertical amplitude effect F_{RV} is expressed as the following equations, which is slightly different from those of domes in F_H.

$$F_H = \begin{cases} 3/2 & (0 < R_T \le 1/4) \\ 1/2\left(\sqrt{1/R_T}+1\right) & (1/4 < R_T \le 1) \\ 1 & (1 < R_T) \end{cases} \quad (14)$$

$$F_V = \begin{cases} 3C_V\theta & (0 < R_T \le 5/16) \\ \left(\sqrt{5/R_T}-1\right)C_V\theta & (5/16 < R_T \le 5) \\ 0 & (5 < R_T) \end{cases} \quad (15)$$

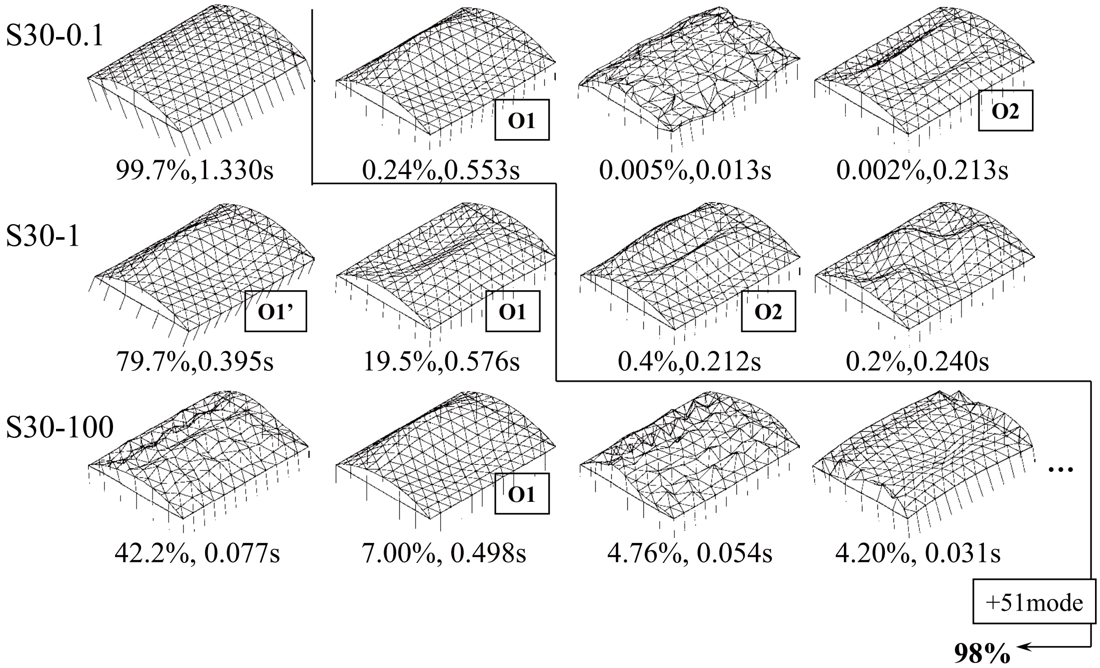

***Figure 18.** Effects of Substructure Stiffness (d10)*

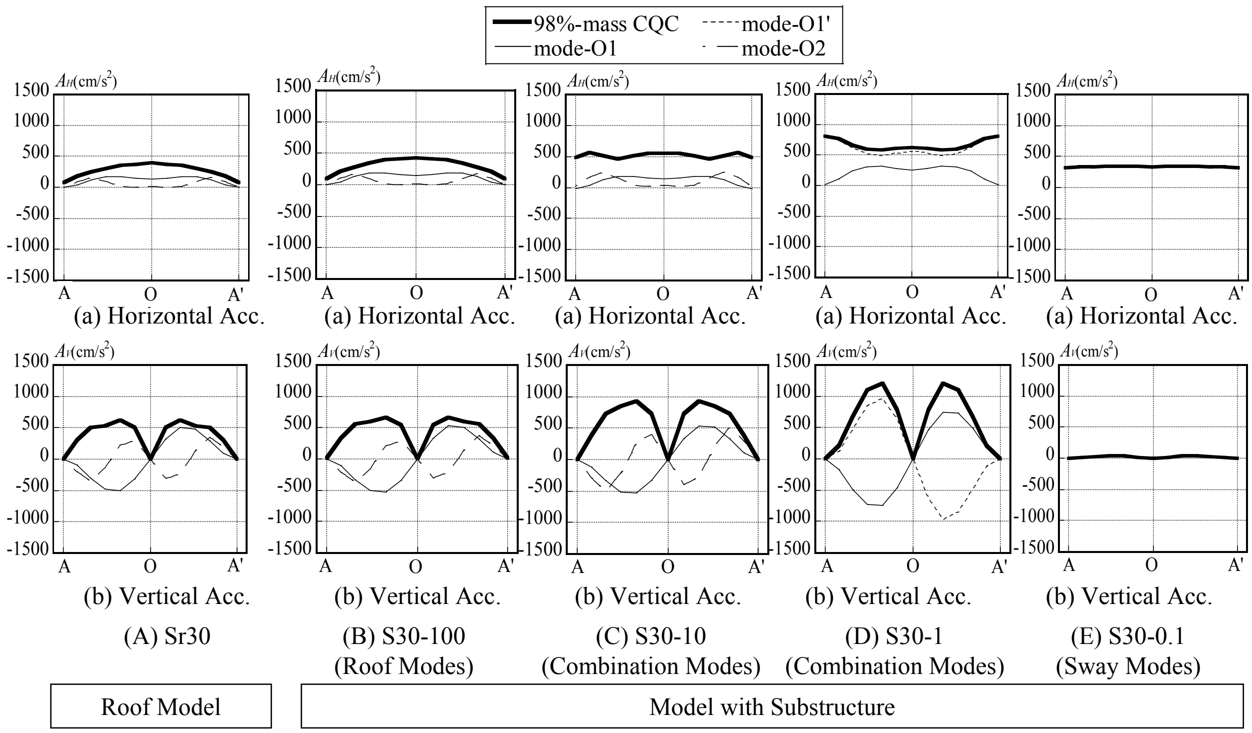

Figure 19. *Components of Each Modes (d10)*

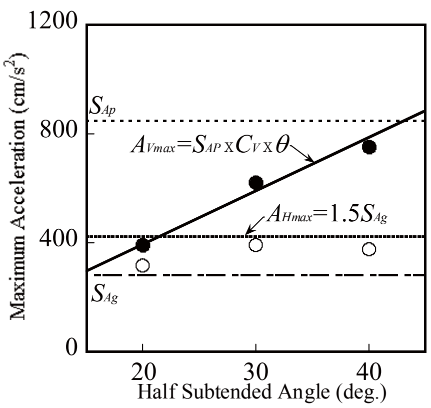

Figure 20. *Components of Each Modes*

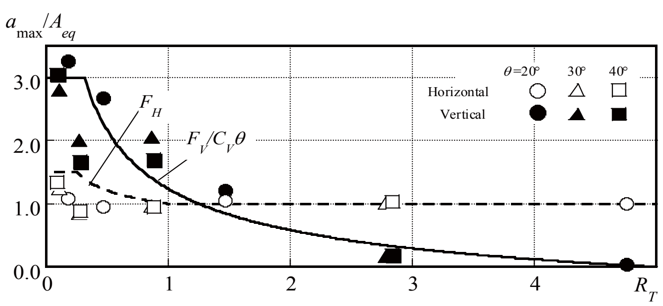

Figure 21. *Amplification Factors for Cylindrical Shells*

From studies with roof models, the maximum acceleration distribution can be expressed as the following equations.

Horizontal acceleration:

$$A_H(x,y) = A_{eq}\left\{1+(F_H-1)\cos\pi\left(\frac{x}{L_x}\right)\cos\pi\left(\frac{y}{L_y}\right)\right\} \quad (16)$$

Vertical acceleration:

$$A_V(x,y) = A_{eq}F_V \sin\pi\left(\frac{2x}{L_x}\right)\cos\pi\left(\frac{y}{L_y}\right) \quad (17)$$

Above distribution is compared with the results of CQC method in Figure 22. The equivalent static loads are delivered as same as domes. The displacements and member forces using these equivalent static loads are compared with the results of CQC method in Figure 23. White marks are the results of d10 series, and black marks are those of d100 series. The results of proposed method are more accurate in roofs with higher out-of-plane stiffness, and considered to be applicable also in cylindrical shells with depth/span ratio over 1/100.

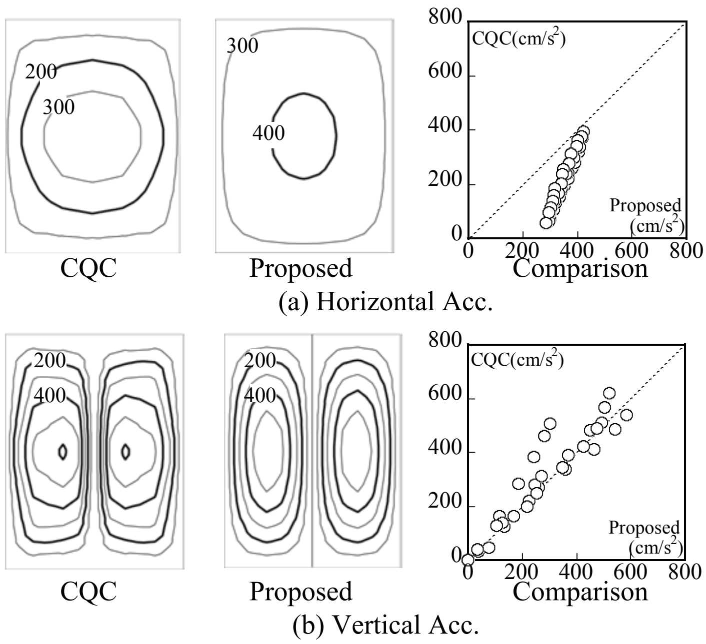

Figure 22. *Acceleration Distribution in Cylindrical Shell (Sr30)*

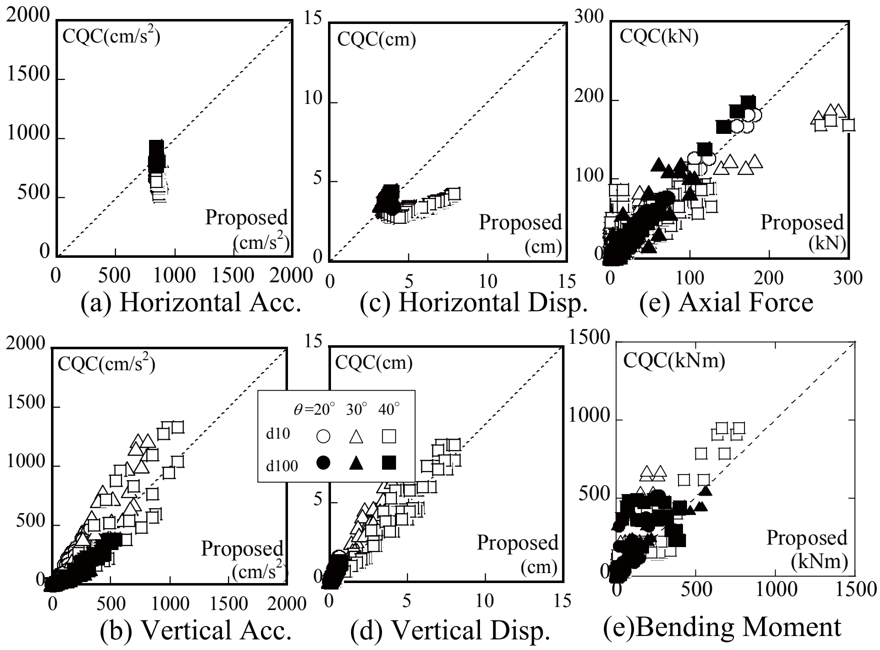

Figure 23. *Accuracies of Proposed Static Load (Sθ-1 series)*

5. EFFECT OF MASS RATIO

Above discussions are under conditions where mass ratio $R_M=M_{eq}/M_R$ is relatively small. However, as indicated in Section 2 and Figure 6, excitation of amplification factors around $R_T=1$ are expected in high R_M cases. In this section, additional indication formulas covering these excitations are discussed.

The similar studies as previous sections are carried out for arches, domes and cylindrical shells with $\theta=30^\circ$ with $R_M=1.2$, 3 and 9. Here, the arch models are defined as removing the end strut from cylindlical shell models, and the results of arches are shown in Figure 24. In this figure, CQC results are indicated as marks, and amplification factors in eq. (9) are indicated in chained lines, and proposed design equations (eq.(14), (15)) are indicated in solid lines. When R_M=1.2, the amplification is covered by proposed design formulas, however with increasing R_M factor, the CQC results and eq.(9) exceeds the solid lines around R_T=1. This condition occurs when the weight of substructures is much higher than the roof, and their natural periods meet each other, as light steel roof sits on multi-story RC buildings, for example. To cover these phenomena, the following equations are proposed.

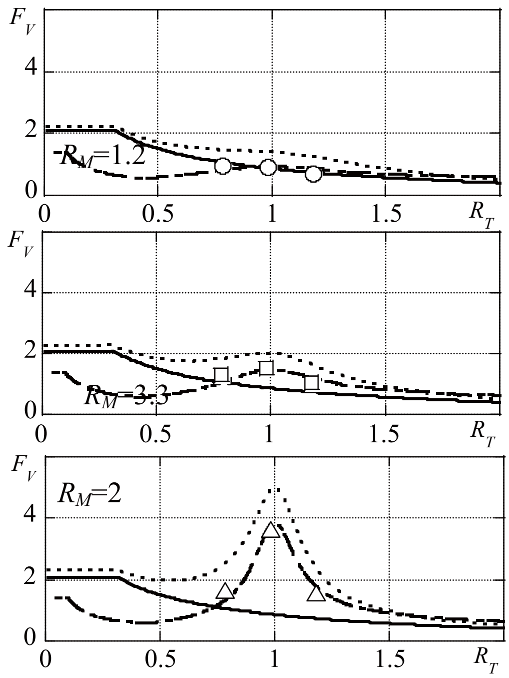

Figure 24. *High R_M Response of Arch*

$$F'_H = \sqrt{F_H^2 + \frac{1}{(1-R_T^2)^2 + (1/R_M)^{\theta}}} \qquad (18)$$

$$F'_V = \sqrt{F_V^2 + \frac{1}{(1-R_T^2)^2 + (1/R_M)}} \qquad (19)$$

Here, θ (rad) is half subtended angle. Modified amplification factors using F_H' and F_V' given by eq.(18) and (19) instead of F_H and F_V are shown in Figure 26 and 27, together with CQC results of cylindrical shells and domes, respectively. Modified formulas are well covers the CQC results, and considered to be valid. These equations will need to be applied where R_M>2 and R_T<1.5.

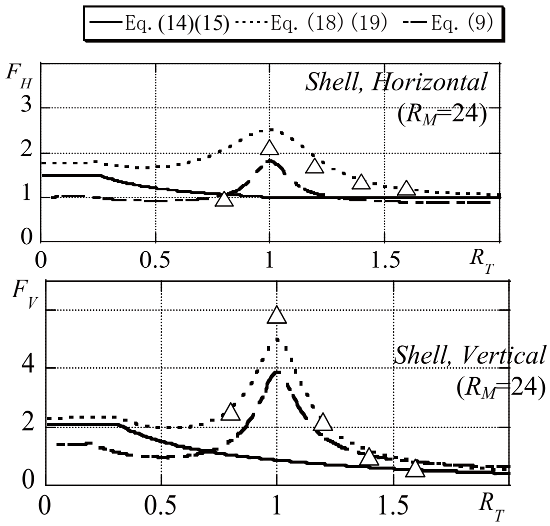

Figure 25. *High R_M Response of Cylindrical Shell*

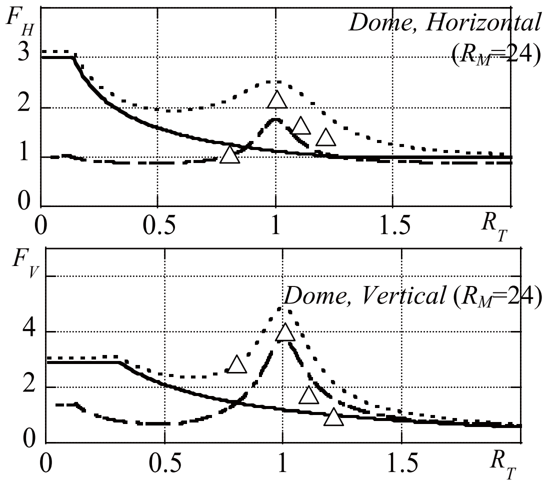

Figure 26. *High R_M Response of Dome*

6. CONCLUSIONS

In this paper, the response characteristics of raised roof as domes and cylindrical shell are expressed by simple equations with parameters of half subtended angle, natural period ratio and mass ratio between the roof and substructures, and their validities are studied and discussed. As results, the followings are obtained.

1) The basic response characteristics of raised roofs can be explained by 3-hinged arch model. The effects of half subtended angles or effects of substructure stiffness are expressed by simple formulas including parameters of half subtended angles, natural period ratio and mass ratio between the roof and substructure.

2) Lattice domes has large numbers of parallel vibration modes, however, numbers of major modes decreases when out-of-plane stiffness increases. Where depth/span ratio >1/50, maximum acceleration distribution in horizontal and vertical directions are expressed by simple amplification factors, which can be used as equivalent static loads.

3) Cylindrical lattice shell roofs has the similar characteristics as domes, and their maximum acceleration distributions are also expressed by simple equations where depth/span ratio >1/100. Their validities are confirmed against the results of CQC method.

4) The depth/span ratio can be calculated by the truss beam depth divided by the roof span for double layer truss roof. Although the proposed method is not likely to be applicable to single layer roofs, the depth/span ratio can be calculated by radius of gyration of the roof member section multiplied by 2 divided by the span.

5) Where the mass ratio R_M>2, excitation in amplification factors are observed around R_T=1 zones. To cover these phenomena, additional design equations are proposed.

With these results, the basic response characteristics of raised roofs are commonly explained along their angle, stiffness, and mass parameters. The proposed method delivers roof accelerations from design shear force of each stories and consistent with contemporary multistory design concepts. Although present studies are discussed under elastic zones, the same approach is considered to be effective where the substructure goes into elasto-plastic zones [11].

Also it is noted that the stability problem due to large deformation is not included in these studies.

REFERENCES

[1] ***Kato, S., Konishi, K., Nakazawa, S.:*** *Push-over analysis and static estimation of seismicresponses of large steel space structures, Comparison of static estimation based on push-over analysis with direct dynamic analysis,* IASS-APCS 2003, Taipei, Taiwan, Oct. 2003, pp.54-55.

[2] ***Kato, S., Nakazawa, S., Saito, K.:*** *Two-mode based estimation of equivalent seismic loads and static estimation of dynamic response of reticular domes supported by ductile substructures,* Journal of IASS, Vol. 47 (2006) n.1, pp.35-52.

[3] ***Yamada, S., Matsumoto, Y., Saito, E.:*** *Static seismic load modelling using continuum shell analogy for single layer latticed cylindrical shell structures,* IASS-APCS 2006, Beijing, China, Oct. 2006, pp.80-81.

[4] ***Yamada, M.:***, *A basic study on the effect of substructures for the seismic response of space structures,* Shell and Spacial Structures Seminar, No.10, AIJ symposium, 2001.11 (in Japanese).

[5] ***Zheng, Z., Yamada., M.***: Seismic response distribution characteristics of arch, AIJ anural meeting procedure, B-1, pp.859, 2000.9 (in Japanese).

[6] ***Guputa, K.:***Response Spectrum Method, CRC Press, 1992.

[7] ***Building Research Center,*** Japan : Method of setting seismic input for building design, 1994.4 (in Japanese).

[8] ***Ogawa, T., Takeuchi, T., Nakagawa, M., Kumagai, T. :*** Seismic response analysis of single layer lattice domes, IASS-APCS 2003, Taipei, Taiwan, Oct. 2003, pp.110-111.

[9] ***Takeuchi,.T., Ogawa, T., Nakagawa, M., Kumagai, T.:*** Response evaluation of medium-span lattice domes with substructures using response spectrum analysis, IASS 2004, Montpellier, France, Oct. 2004, pp.205-206.

[10] ***Takeuchi,.T., Ogawa, T., Kumagai, T.:*** Response evaluation of cylindrical lattice shell roofs with substructures using response amplification factors, IASS 2005, Bucharest, Rumania, Oct. 2005, pp.383-390.

[11] ***Kumagai, T., Takeuchi,.T., Ogawa, T.:*** Response evaluation of lattice domes with substructures using response amplification factors, IASS 2005, Bucharest, Rumania, Oct. 2005, pp.391-398.